Age of mineralization in the Luis Lopez manganese district, Socorro County, New Mexico, as determined by $^{40}Ar/^{39}Ar$ dating of cryptomelane

Virgil W. Lueth, Richard M. Chamberlin, and Lisa Peters
New Mexico Bureau of Geology and Mineral Resources, New Mexico Institute of Mining and Technology, Socorro, NM 87801

Abstract

Cryptomelane, $K(Mn^{4+},Mn^{2+})_8O_{16}$, samples from the Nancy and MCA mines in the Luis Lopez manganese district were collected in order to determine the age of mineralization using the $^{40}Ar/^{39}Ar$ dating method. Cryptomelane precipitation occurred at the onset of calcite mineralization following banded manganese ore deposition. X-ray diffraction analysis confirmed sample composition and purity. $^{40}Ar/^{39}Ar$ dating of two cryptomelane samples from the MCA mine and one from the Nancy mine yielded age spectra with generally increasing radiogenic yields and apparent ages that suggest Ar loss. The apparent ages of the oldest furnace analysis heating steps from the MCA-2 sample (6.69 ± 0.04 Ma) and 9189 from the Nancy mine (6.33 ± 0.04 Ma) are assigned as minimum ages of mineralization. These ages are consistent with age estimates for mineralization (ca 3–7 Ma) based on geologic relationships in the area as established by previous workers.

These age determinations indicate manganese mineralization closely followed regional potassic metasomatism. Published $^{40}Ar/^{39}Ar$ ages of metasomatic adularia from jasperized fanglomerates north of the Nancy mine indicate metasomatism persisted until at least 7.4 Ma. Minor manganese veins near the Nancy mine cut jasperized fanglomerates and cut numerous jasper veinlets in the Oligocene tuffs affected by this earlier alteration. A published model for the Luis Lopez district previously interpreted the mineralization to be derived from a manganese-depleted red alteration zone superimposed on thick intracaldera tuff (31.9 Ma) near the center of the district. A dike dated at 11.05 ± 0.05 Ma is unaltered where it cuts across the southern arm of the red zone. This indicates that the red zone is at least 4.4 m.y. older than manganese mineralization at the MCA and Nancy mines and genetically unrelated. A composite upper-crustal silicic pluton is inferred to have fed episodic eruptions of dacitic and rhyolitic lava domes (at 9.5, 8.7, 7.8, 7.5, and 7.0 Ma) in the Socorro Peak area, 8–9 km northeast of the Nancy mine. This plutonic complex represents the most likely heat source for the hydrothermal system of the Luis Lopez manganese district. Miocene playa claystones formed an impermeable cap to the hydrothermal system, thereby forcing significant lateral flow (i.e., 9 km) of the mineralizing waters.

Introduction

Direct dating of hydrothermal ore mineralization has been the focus of extensive research since the discovery of radiometric age dating techniques. However, most deposits contain ore minerals that are not amenable to these methods. Manganese mineralization in the study area contains cryptomelane, $K(Mn^{4+},Mn^{2+})_8O_{16}$, a potassium-bearing phase that was successfully dated by K-Ar methods as early as 1966 (Chuchrov et al. 1966). Subsequently, the $^{40}Ar/^{39}Ar$ technique has been applied to a number of potassium-bearing manganese minerals with varying success (Vasconcelos 1999, 2000). Most geochronological studies have focused on residual (lateritic) manganese ore deposits rather than hydrothermal types. To our knowledge this study represents one of the first attempts at the dating of hydrothermal manganese minerals.

Mining of vein type hydrothermal manganese mineralization in the Luis Lopez manganese district (Fig. 1) began during the First World War and continued sporadically until the early 1970s. Ore was mined from the steeply dipping vein systems via underground workings and open cuts. Earlier geological studies in the district were made by Miesch (1956), Farnham (1961), Hewett (1964), Willard (1973), Chamberlin (1980), and Eggleston (1982). Fluid inclusion studies by Norman et al. (1983) detailed hydrothermal characteristics of the district. A study by Eggleston et al. (1983b) combined alteration patterns with geologic, geochemical, and oxygen isotope data in the development of a genetic model for the manganese deposits. Geologic maps of the Luis Lopez quadrangle (Chamberlin and Eggleston 1996; Chamberlin et al. 2002) and the Socorro quadrangle (Chamberlin 1999) provide basic field relationships in the study area. This information is now augmented by numerous new $^{40}Ar/^{39}Ar$ age dates on volcanic strata, intrusions, and potassium metasomatized rocks (cf. Newell et al. 1996; Dunbar et al. 1996; Chamberlin et al. 2004 this volume). This paper presents the results of $^{40}Ar/^{39}Ar$ dating of three cryptomelane samples from Luis Lopez district and compares these results with data from previous studies.

Geology

Steeply dipping calcite-manganese oxide veins exposed in the northern and central Chupadera Mountains comprise the Luis Lopez manganese district located approximately 15 km southwest of the town of Socorro in central New Mexico (Fig. 1). The Chupadera range represents an east-tilted extensional fault block uplift of the central Rio Grande rift. In the Socorro–Magdalena area of the Rio Grande rift, 29 m.y. of progressive crustal extension has broken an Oligocene caldera cluster and surrounding volcanic plateau into a north-trending series of tilted-fault-block uplifts and intervening alluvial basins (Chapin and Cather 1994). Primary host rocks for north-striking veins of the Luis Lopez manganese district are densely welded intracaldera tuffs of late Oligocene age (31.9–27.9 Ma) within the eastern sector of the Socorro caldera and along the eastern topographic wall of the younger Sawmill Canyon caldera, which is partially exposed near the Nancy mine (Chamberlin and

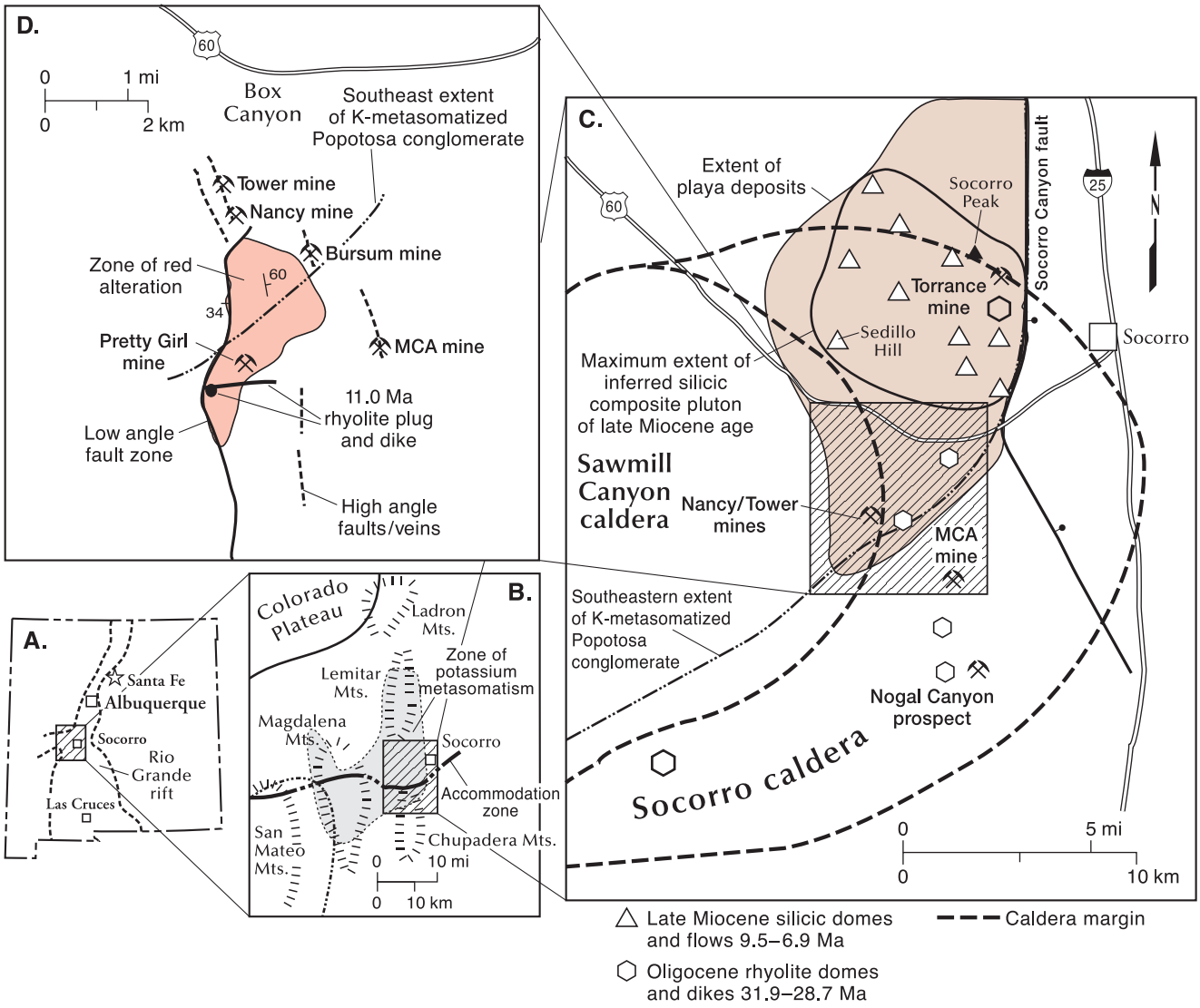

FIGURE 1—Series of location maps illustrating pertinent geologic features within the study area. **A**–Location of the study area with respect to the Rio Grande rift (modified from Dunbar et al. 1994). **B**–Extent of regional potassium metasomatism (> 6% K_2O) derived from flight lines of the NURE aerial radiometric and magnetic survey (U.S. Dept. of Energy 1979a,b). **C**–Distribution of playa lake deposits and Oligocene–Miocene silicic volcanic vents in the study area (from Chamberlin 1999; Chamberlin et al. 2004 this volume). **D**–Map of red zone alteration and some manganese deposits in the study area. (modified from Eggleston et al.1983a).

Eggleston 1996; Chamberlin et al. 2002; Chamberlin et al. 2004 this volume). The northeastern topographic wall of the Socorro caldera is partially exposed in the west-tilted Socorro Peak uplift, about 10 km northeast of the Luis Lopez district.

In middle to late Miocene time, locally derived volcanic-rich conglomerates and intertonguing playa mudstones unconformably buried Oligocene volcanic rocks and associated caldera structures in the Chupadera–Socorro Mountains area (Cather et al. 1994; Chamberlin 1999). Six distinct episodes of small volume trachyandesite to rhyolite lava flows and domes were erupted onto an aggrading playa floor near Socorro Peak between 9.5 and 6.9 Ma. Four well-dated episodes of rhyolite extrusion occurred at 8.7, 7.8, 7.5, and 7.0 Ma (Newell et al. 1996). In the Pound Ranch area approximately 5 km west of the Tower mine, dacite and rhyolite lava domes were erupted directly onto faulted and uplifted Oligocene volcanic rocks at about 11.3 Ma (Osburn et al. 1986; Newell et al. 1996). Similar dacitic lavas (ca 11–12 Ma) locally overlap Miocene conglomerates and Oligocene tuffs just north of the Tower mine (Chamberlin et al. 2002).

Faulting is complex and pervasive in the district. Caldera related faults and north-trending early rift faults have been rotated about 40–50° to the east in the southern and central part of the manganese district near the MCA mine (Chamberlin et al. 2002). Strong rotation of fault blocks in the rift is attributed to progressive domino-style crustal extension, which began about 29 m.y. ago (Chamberlin 1983; Cather et al. 1994). An area of red alteration within the uplifted and east-tilted caldera-facies Hells Mesa Tuff (Fig. 1) is truncated along its western margin by a large low-angle rift fault that dips about 30° to the west (Chamberlin et al. 2002). Steeply dipping manganese-calcite veins at the MCA and Nancy/Tower mines appear to post date most of the fault block rotation that occurred in late Oligocene and Miocene time. These geologic and structural constraints originally placed the age of mineralization between 7 and 3 Ma (Chamberlin 1980; Eggleston et al. 1983a). Additional discussion of the regional structural setting can be found in Chamberlin et al. (2004 this volume).

No specific intrusive body has been identified in direct relationship with the formation of the manganese deposits

in the Luis Lopez district. East-trending crystal-poor rhyolite dikes that cut caldera-facies tuff south of the Nancy mine and a coarsely porphyritic rhyolite plug/dike about 4 km west of the MCA mine were considered to represent possible heat sources, as well as late Miocene rhyolite domes near Socorro Peak (Eggleston et al. 1983). Recent $^{40}Ar/^{39}Ar$ dating indicates the crystal-poor dikes are of late Oligocene age (~ 28.7 Ma) and a coarsely porphyritic plug (Chamberlin et al. 2004 this volume) and an associated dike are of late Miocene age (11.0 Ma), respectively.

Alteration

Eggleston et al. (1983) recognized two types of alteration in the Luis Lopez district. They include the southeastern margin of a regional zone of potassium metasomatism that is widely exposed in several mountain ranges of the Socorro–Magdalena area (Fig. 1). A much smaller zone of "red alteration" confined to lower caldera-facies Hells Mesa Tuff in the central part of the district (Fig. 1) represents the second type. A third type of alteration, carbonatization, is locally associated with manganese oxide mineralization.

Regional potassium metasomatism

Regional potassium metasomatism is of middle to late Miocene age (Dunbar et al. 1994; Dunbar and Miggins 1996). Early rift fanglomerates within the broad zone of potassium metasomatism are an anomalous red color and very well indurated (Chapin and Lindley 1986). Metasomatism commonly extends a kilometer or more into the underlying Oligocene volcanic pile. Metasomatized rocks are characterized by potassium feldspar (mainly adularia) that has preferentially replaced plagioclase; they contain as much as 12 wt% K_2O (Chapin and Lindley 1986; Ennis et al. 2000). Initially, regional potassium metasomatism was interpreted as the expression of a large geothermal system (D'Andrea-Dinkelman et al. 1983). More recently, the giant K_2O anomaly has been attributed to downward percolation of alkaline basin brines from a large playa system of Miocene age (Chapin and Lindley 1986; Dunbar et al. 1994).

In the northern Chupadera Mountains fanglomerates of Miocene age that are potassium metasomatized are also anomalously well indurated by jasperoidal silica (Chamberlin and Eggleston 1996; Ennis 1996). Jasperized fanglomerates occur approximately 2 km southwest and 3 km east of the Nancy mine but do not extend as far south as the MCA mine. Metasomatic adularia hand picked from clasts in jasperized conglomerates approximately 3 km north of the Nancy mine yield $^{40}Ar/^{39}Ar$ ages of 8.7 ± 0.1 and 7.4 ± 0.1 Ma (Dunbar and Miggins 1996). Minor manganese veins near the Nancy mine cut jasperized conglomerates and also cut numerous jasper veinlets in the underlying Oligocene tuffs.

Red zone alteration

Another alteration event, "red zone alteration," (Fig. 1) was interpreted to be superimposed on the potassium metasomatism zone and directly related to manganese mineralization (Eggleston et al. 1983a). Alteration in the red zone is characterized by the destruction of ferromagnesian minerals (biotite and hornblende) and subsequent formation of opaque oxides and sericite. Feldspars are partially altered to clays and sericite, and the groundmass is reddened by hematite. Manganese is depleted in the red zone, and by inference, reconcentrated in the veins around the zone (Eggleston et al. 1983a). However, manganese mineralization is locally present within the red zone along fractures and faults (e.g., Pretty Girl mine; Willard 1973).

Carbonatization

Alteration directly associated with vein and breccia manganese mineralization is dominated by calcite. Manganese oxide and calcite veins consistently crosscut jasperoidal conglomerates and veinlets in addition to K-metasomatized rocks in the district (Chamberlin and Eggleston 1996). Manganese veins at the north end of the MCA mine cut Hells Mesa Tuff that contains metasomatic adularia, as documented by X-ray diffraction analysis (Hewett 1964). Interestingly, alteration selvages are notably absent adjacent to mineralized veins in the metasomatized rocks. Calcite, however, locally replaces plagioclase outside the margins of veins just south of the MCA mine (Chamberlin and Eggleston 1996).

Mineralization

Mineralization is hosted by the 31.9 Ma Hells Mesa Tuff at the MCA mine. The 27.9 Ma Lemitar Tuff and underlying volcaniclastic rocks of the Sawmill Canyon Formation serve as host rocks at the Nancy/Tower mines (age data from Chamberlin et al. 2004 this volume). The form of the deposits is both as vein breccias and near vertical lenticular veins in the brittle, densely welded rhyolite tuffs. Ores consist of banded manganese oxides with calcite and variable, but minor amounts, of quartz (crystal and chalcedony). Minor manganese-calcite veins at the Nogal Canyon prospect occur in an 8.4 Ma basalt flow near Walnut Creek, approximately 4 km south of the MCA mine (Chamberlin et al. 2002). Gently tilted early Pliocene (?) piedmont-slope gravels of the lower Sierra Ladrones Formation unconformably overlie late Miocene playa deposits of the Popotosa Formation (ca 9.5–6.9 Ma) near the west margin of the Socorro Basin, approximately 4 km east of the Nancy mine. A 30-cm-thick gravel bed in the lower Sierra Ladrones near this locality is unusually well cemented by black manganiferous silica and calcite. This minor occurrence may represent the last gasp of mineralization related to the Luis Lopez district (Chamberlin and Eggleston 1996).

All ore mineralization in the district occurs as open space filling. The sequence of manganese oxide precipitation from the walls to the centers of the veins and breccias varies from deposit to deposit, even within a single hand specimen (Willard 1973). Norman et al. (1983) developed a general paragenesis for the district (Fig. 2). Apparently, deposition of all manganese ore minerals was essentially simultaneous. Depositional patterns, reflected by alternating layers of manganese oxides and calcite, often repeat during the course of mineralization. Calcite veining tends to post-date manganese mineralization. Ore mineralization, determined by X-ray diffraction, consists mainly of cryptomelane-group minerals: coronadite ($PbMn_8O_{16}$), cryptomelane [$K(Mn^{4+},Mn^{2+})_8O_{16}$], and hollandite ($BaMn_8O_{16}$). Other manganese oxide phases include: pyrolusite (MnO_2), and chalcophanite ($(Zn,Fe,Mn)\ Mn_3O_7 \cdot 3\ H_2O$).

During the course of this study, a particular paragenetic relation was established for cryptomelane. The most abun-

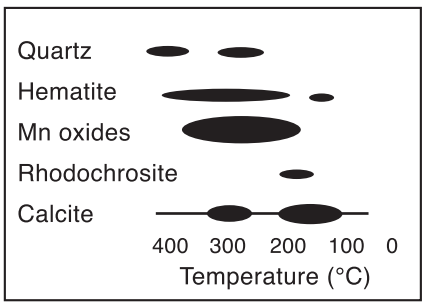

FIGURE 2—Generalized mineral paragenesis for the Luis Lopez manganese district as adapted from Norman et al. (1983).

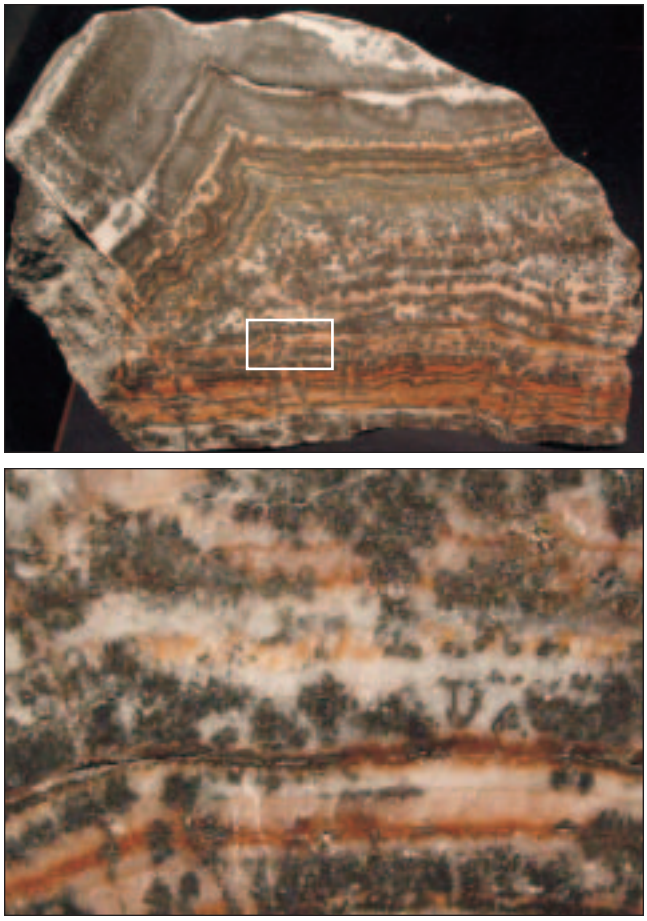

FIGURE 3—Photographs of mineralization features at the Nancy mine. **A**–Sample from the Nancy mine, long dimension is 25 cm. **B**–Close-up of the arborescent growths of cryptomelane needles projecting into calcite.

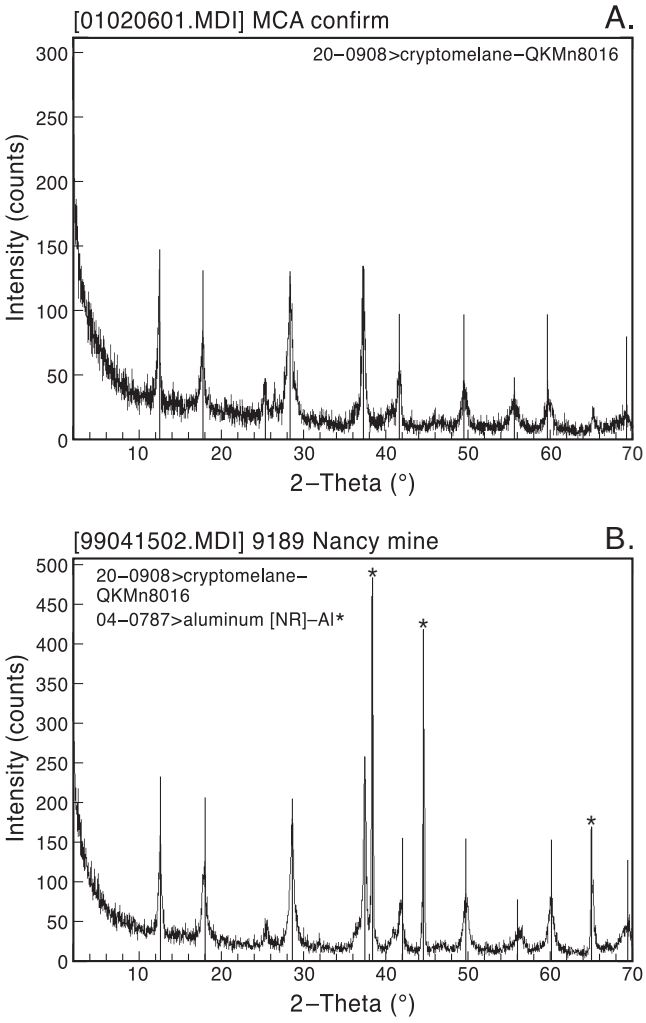

FIGURE 4—X-ray diffraction spectra for samples analyzed from: **A**–the MCA mine and **B**–the Nancy mine. Standard powder diffraction file X-ray spectra superimposed on sample pattern.

dant occurrence of cryptomelane is at the manganese oxide-calcite interface within any manganese oxide-calcite mineralization band (Fig. 3). Cryptomelane occurs as dendritic masses composed of needles projecting into pure, white calcite bands. Apparently, cryptomelane deposition is favored at the conditions of initial calcite precipitation in these ores. Needles of cryptomelane were also present in black calcite, similar to those described by Willard (1973).

Norman et al. (1983) documented the hydrothermal nature of these deposits by fluid inclusion studies. The temperatures of deposition for the ores are estimated to range predominantly between 225 and 325°C, based on fluid inclusion homogenization temperatures. Average homogenization temperatures are generally higher, 275–325°C, in the northern part of the district compared to those farther south at the MCA mine, 225–275°C. Most of the fluid inclusions were found to be vapor-rich, indicative of boiling conditions. Freezing determinations on the inclusions indicated low salinities around 0 wt.% equivalent NaCl. Gas analysis by Norman et al. (1983) indicated the vapors were dominated by CO_2, and that H_2S was absent.

Analytical methods and results

Manganese ore samples were collected at the Tower / Nancy and MCA mines. Mineralogy was determined by a combination of petrographic analysis and X-ray diffraction. Standard powder mounts were employed, and X-ray diffraction scans were taken over a range of 2–70° 2θ. Pattern comparison was accomplished using Jade software and standard PDF patterns. The resulting X-ray patterns were determined to be almost pure, crystalline cryptomelane with little or no contamination by other manganese oxides (Fig. 4). These patterns are consistent with high K cryptomelane described by Vasconcelos (2000), which is highly amenable to $^{40}Ar/^{39}Ar$ age dating.

Three cryptomelane samples (MCA-1, MCA-2, and 9189) were analyzed by the $^{40}Ar/^{39}Ar$ method using an incremental-heating, age-spectrum technique. Incremental heating was achieved with a Mo double-vacuum resistance furnace, or a 50 watt Synrad CO_2 laser using a beam integrator lens. Samples MCA-2 and 9189 (Nancy mine) were analyzed using both methods to test sample reproducibility and the suitability of each method of gas extraction for cryptomelane. In addition, sample MCA-2, which initial work had shown to be fairly well behaved, was vacuum encapsulated before irradiation to evaluate the potential of ^{39}Ar recoil loss during irradiation. Following irradiation, the encapsulation tube was loaded into the CO_2 laser chamber, the tube punctured with the laser, and the trapped gas analyzed. The sample was then removed from the encapsulation tube and analyzed with the CO_2 laser. Abbreviated analytical methods for the dated samples are given in Table 1, and detailed analytical data are provided in Table 2.

The six age spectra generated from the Luis Lopez cryptomelane (Figs. 5A–F and Table 2) reveal increasing radi-

TABLE 1—Summary of $^{40}Ar/^{39}Ar$ data and analytical methods.

Sample	Unit/location	Irradiation	Mineral	Analysis	No. of steps/ crystals	MSWD	Age	±2σ	Comments
MCA-2	MCA mine	NM-123	cryptomelane	furnace step-heat			6.69	0.04	minimum age
MCA-1	MCA mine	NM-123	cryptomelane	furnace step-heat			6.71	0.04	minimum age
9189 Nancy mine	Nancy mine	NM-123	cryptomelane	furnace step-heat			6.33	0.04	minimum age
RC-KM-28	Red Canyon dike	NM-152	sanidine	laser total fusion	14	2.9**	11.05	0.05	

****** MSWD outside 95% confidence interval

Notes:

Sample preparation and irradiation:

Mineral separates were prepared using standard crushing, dilute acid treatment, and hand-picking techniques.

Cryptomelane separates were loaded into a machined Al disc and irradiated for 24 hrs in L-67 position, Ford Memorial Reactor, University of Michigan.

Sanidine was loaded into a machined Al disc and irradiated for 14 hrs in D-3 position, Nuclear Science Center, College Station, TX.

Neutron flux monitor Fish Canyon Tuff sanidine (FC-1). Assigned age = 27.84 Ma (Deino and Potts, 1990) relative to Mmhb-1 at 520.4 Ma (Samson and Alexander 1987).

Instrumentation:

Mass Analyzer Products 215-50 mass spectrometer on line with automated all-metal extraction system.

Cryptomelane separates were step-heated using both a Mo double-vacuum resistance furnace and a 50 watt Synrad CO_2 laser using a beam integrator lens. Heating duration in the furnace 9 min.

Reactive gases removed during furnace analysis by reaction with 3 SAES GP-50 getters, two operated at ~ 450°C and one at 20°C. Gas also exposed to a W filiment operated at ~ 2000°C.

Heating duration for samples step-heated with a 50 watt CO_2 laser using a beam integrator lens was 3 min.

Reactive gases removed by reaction with two SAES GP-50 getters, one operated at ~ 450°C and one at 20°C for 30 or 40 min. Gas also exposed to a W filament operated at ~ 2000°C and a cold finger operated at – 140°C.

Single crystal sanidine were fused by a 50 watt Synrad CO_2 laser.

Reactive gases removed during a 2 min reaction with two SAES GP-50 getters, one operated at ~ 450°C and one at 20°C. Gas also exposed to a W filament operated at ~ 2000°C and a cold finger operated at –140°C.

Analytical parameters:

Electron multiplier sensitivities: 3.40 x 10^{-16} moles / pA for furnace step-heat, 1.88 x 10^{-16} moles / pA for laser step-heat for L#s 50219-02 and 50226-02, 6.99 x 10^{-17} and 7.10 x 10^{-17} for L#52167-10, 1.23 x 10^{-16} for laser total fusion.

Total system blank and background for the furnace averaged 1790, 7.9, 1.5, 1.3, 7.0 x 10^{-18} moles; 296, 21, 5.1, 0.8, 1.2 x 10^{-18} moles for the laser step-heat and 902, 0.64, 0.40, 1.7, and 1.2 x 10^{-18} moles for laser fusion at masses 40, 39, 38, 37, and 36, respectively.

J-factors determined to a precision of ± 0.1% by CO_2 laser-fusion of 4 single crystals from each of 3 or 4 radial positions around the irradiation tray.

Correction factors for interfering nuclear reactions were determined using K-glass and CaF_2 and are as follows:

$(^{40}Ar/^{39}Ar)_K = 0.0225 \pm 0.00015$; $(^{36}Ar/^{37}Ar)_{Ca} = 0.000278 \pm 0.000006$; and $(^{39}Ar/^{37}Ar)_{Ca} = 0.000727 \pm 0.000002$ for NM-104

$(^{40}Ar/^{39}Ar)_K = 0.0257 \pm 0.0013$; $(^{36}Ar/^{37}Ar)_{Ca} = 0.00027 \pm 0.00002$; and $(^{39}Ar/^{37}Ar)_{Ca} = 0.0007 \pm 0.00005$ for NM-136

$(^{40}Ar/^{39}Ar)_K = 0.0002 \pm 0.0003$; $(^{36}Ar/^{37}Ar)_{Ca} = 0.00028 \pm 0.000005$; and $(^{39}Ar/^{37}Ar)_{Ca} = 0.0007 \pm 0$ .00002 for NM-152.

Age calculations:

Integrated age and error calculated by weighting individual steps by the fraction of 39Ar released.

Plateau age is inverse-variance-weighted mean of selected steps.

Plateau age is inverse-variance-weighted mean error (Taylor, 1982) times root MSWD where MSWD>1.

Plateau and integrated ages incorporate uncertainties in interfering reaction corrections and J factors.

MSWD values are calculated for n-1 degrees of freedom for weighted mean age.

$^{40}Ar/^{36}Ar$, and MSWD values calculated from regression results obtained by the methods of York (1969).

If the MSWD is outside the 95% confidence window (cf. Mahon, 1996; Table 1), the error is multiplied by the square root of the MSWD.

Decay constants and isotopic abundances after Steiger and Jäger (1977).

All final errors reported at ±2σ, unless otherwise noted.

ogenic yields and in general increasing apparent ages throughout most of the ^{39}Ar released. This effect is less pronounced for MCA-2 than it is for either MCA-1 or 9189. It is also noted that the laser analyses of MCA-2 and 9189 show the effect to a lesser degree and do not reach as old an apparent age as the furnace analyses. The maximum ages revealed (except for the highest temperature steps that contain only a few percent of the ^{39}Ar released) by the furnace analyses of the MCA samples are 6.69 ± 0.04 Ma (MCA-2) and 6.71 ± 0.04 Ma (MCA-1), whereas that of sample 9189 is slightly younger, 6.33 ± 0.04 Ma.

The ^{39}Ar recoiled into the encapsulation tube of MCA-2 accounted for 2.7% of the ^{39}Ar released from this sample. When this gas is added into the integrated age of the standard step-heat analysis (6.23 ± 0.18 Ma), the resultant age (5.96 ± 0.30 Ma) is within error.

Fourteen single sanidine crystals (RC-KM-28) from a rhyolite dike were analyzed by the single-crystal laser fusion method. A weighted mean age of 11.05 ± 0.05 Ma was calculated from the 14 crystals (Fig. 6). The age data are displayed on a probability distribution diagram (Deino and Potts 1990). Abbreviated analytical methods for the dated samples are given in Table 1. The argon isotopic results are summarized in Table 1, and details of the analysis are listed in Table 3.

Discussion

$^{40}Ar/^{39}Ar$ cryptomelane dating results

The dated cryptomelane samples exhibit characteristics desirable for argon age dating; a high degree of crystallinity, large grain sizes, and a high degree of purity (Vasconcelos 2000). In addition, the small amount of ^{39}Ar released into the encapsulation tube of sample MCA-2 (< 3% of the total ^{39}Ar released by this sample) suggests that ^{39}Ar recoil is not a problem for this type of cryptomelane. However, as mentioned above, all of the Luis Lopez cryptomelane age spectra reveal increasing radiogenic yields correlated with increasing apparent ages that are suggestive of Ar loss. The apparent ages of the oldest and most radiogenic heating steps from the furnace analyses have therefore been

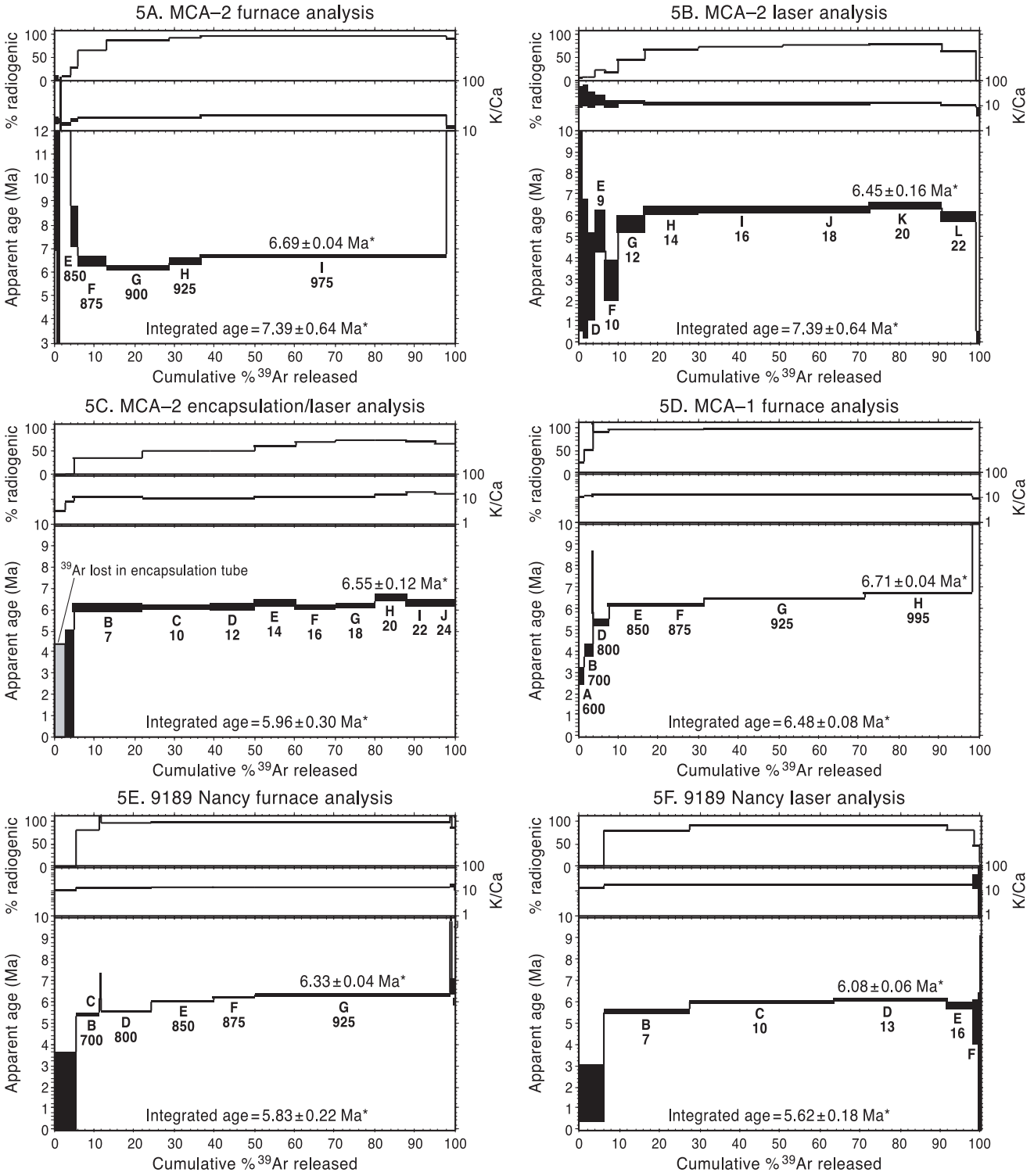

FIGURE 5—Age spectra from the MCA and Nancy ore. **5A**–MCA-2 furnace step-heating analysis; **5B**–MCA-2 laser step-heating analysis; **5C**–MCA-2 sample vacuum encapsulated before irradiation and step-heated with laser. ^{39}Ar recoiled into encapsulation tube shown by unfilled box. **5D**–MCA-1 furnace step-heating analysis. **5E**–Nancy mine 9189 furnace step-heating analysis. **5F**–Nancy mine 9189 laser step-heating analysis. Minimum ages for mineralization assigned to maximum apparent ages of furnace analyses. * 2σ

assigned as the minimum ages of mineralization for samples MCA-2, MCA-1, and 9189 (6.69 ± 0.04 Ma, 6.71 ± 0.04 Ma, and 6.33 ± 0.04 Ma, respectively). It is thought that the laser analyses are more concordant than the furnace analyses due to uneven heating and thus homogenization of the Ar extracted from the cryptomelane. It is noted that the ages assigned to the MCA samples agree within error, whereas the Nancy mine cryptomelane (9189) yielded a slightly younger age. It is unlikely that these samples have been reheated to temperatures greater than their temperatures of formation, 225–325°C. This type of loss spectra has also been seen in lateritic cryptomelane from West Africa that is also very unlikely to have undergone reheating (Hénocque et al. 1998). Vasconcelos (2000) has found in thermogravimetric

TABLE 2—Argon isotopic data for furnace and laser step-heating analysis. Isotopic ratios corrected for blank, radioactive decay, and mass discrimination, not corrected for interfering reactions. Individual analyses show analytical error only; total gas age errors include error in J and irradiation parameters. **n** = number of heating steps; **K/Ca** = molar ratio calculated from reactor produced $^{39}Ar_K$ and $^{37}Ar_{Ca}$; ***** = 2σ error; **D** = mass spectrometer discrimination value. Ages in bold text assigned as mininum ages.

ID	Temp (°C)/watts	$^{40}Ar/^{39}Ar$	$^{37}Ar/^{39}Ar$	$^{36}Ar/^{39}Ar$	$^{39}Ar_K$ (x 10^{-3})	K/Ca (x 10^{-16} mol)	$^{40}Ar^*$ (%)	^{39}Ar (%)	Age (Ma)	±1σ (Ma)
MCA-2, 7.16 mg cryptomelane, J = 0.0032679, D = 1.00661, NM-104, Lab# = 50219-01										
A	600	373.2	0.0321	1238.3	26.7	15.9	2.0	0.7	42.55	17.81
B	700	212.3	0.0325	711.5	32.2	15.7	1.0	1.6	12.29	10.11
C	750	164.1	-0.0046	534.2	9.50	-	3.8	1.9	36.15	10.09
D	800	44.22	0.0362	138.5	80.5	14.1	7.4	4.1	19.15	2.22
E	850	4.643	0.0326	11.08	69.9	15.7	29.2	6.0	7.94	0.43
F	875	1.666	0.0279	1.851	259.5	18.3	66.9	12.9	6.47	0.11
G	900	1.232	0.0281	0.5278	570.6	18.2	87.3	28.5	6.22	0.05
H	925	1.193	0.0284	0.2436	292.3	18.0	94.1	36.4	6.48	0.07
I	975	1.193	0.0256	0.1230	2252.3	19.9	97.1	97.7	**6.69**	**0.02**
J	1100	2.401	0.0449	0.7208	76.0	11.4	91.3	100.0	12.75	0.31
total gas age			n=10		3669.5	18.9			7.41	0.70*
MCA-2, 4.86 mg cryptomelane, J = 0.0032679, D = 1.00676, NM-104, Lab# =5 0219-02										
A	1	103.7	-0.0148	360.7	4.95	-	-2.8	0.3	-16.91	8.88
B	3	36.13	0.0240	118.9	14.0	21.3	2.8	1.1	5.91	2.68
C	5	10.66	0.0200	34.01	23.3	25.5	5.6	2.4	3.52	1.63
D	7	7.274	0.0294	22.78	29.7	17.3	7.3	4.1	3.13	1.01
E	9	3.981	0.0338	10.40	44.3	15.1	22.5	6.6	5.25	0.49
F	10	3.106	0.0456	8.779	53.4	11.2	16.1	9.7	2.93	0.48
G	12	2.230	0.0409	4.276	118.4	12.5	43.1	16.5	5.59	0.21
H	14	1.605	0.0465	1.790	238.2	11.0	66.9	30.1	6.23	0.11
I	16	1.460	0.0454	1.298	364.8	11.2	73.7	50.9	6.23	0.07
J	18	1.429	0.0462	1.172	382.9	11.0	75.8	72.8	6.27	0.07
K	20	1.406	0.0445	0.9887	313.0	11.5	79.3	90.7	**6.45**	**0.08**
L	22	1.609	0.0485	1.984	149.0	10.5	63.5	99.2	5.93	0.13
M	24	12.84	0.0970	45.02	13.9	5.3	-3.5	100.0	-2.66	1.58
total gas age			n=13		1749.7	11.6			5.86	0.42*
MCA-2, 14.99 mg cryptomelane, J = 0.0038622, D = 1.0042, NM-136, Lab# = 52167-10										
AA	0	57.56	0.1361	195.6	91.7	3.7	0.1	2.7	0.24	2.06
A	3	35.17	0.0667	118.1	69.2	7.7	1.0	4.7	2.36	1.33
B	7	2.494	0.0373	5.405	588.3	13.7	35.6	21.8	6.11	0.09
C	10	1.677	0.0456	2.638	595.6	11.2	53.1	39.1	6.10	0.06
D	12	1.680	0.0477	2.635	372.7	10.7	53.3	49.9	6.13	0.07
E	14	1.493	0.0378	1.918	347.8	13.5	61.7	60.0	6.29	0.07
F	16	1.266	0.0378	1.239	355.3	13.5	70.8	70.3	6.11	0.05
G	18	1.196	0.0372	0.9466	327.3	13.7	76.4	79.8	6.22	0.05
H	20	1.292	0.0320	1.110	273.4	16.0	74.4	87.8	**6.55**	**0.06**
I	22	1.258	0.0260	1.113	246.7	19.6	73.5	95.0	6.30	0.06
J	24	1.359	0.0306	1.460	173.6	16.7	67.9	100.0	6.29	0.08
total gas age			n=11		3441.5	13.3			5.97	0.30*
MCA-1, 11.25 mg cryptomelane, J = 0.0032665, D = 1.00661, NM-104, Lab# = 50218-01										
A	600	2.115	0.0420	5.509	132.0	12.2	22.7	1.4	2.80	0.20
B	700	1.339	0.0406	2.181	169.7	12.6	51.7	3.2	4.01	0.14
C	750	0.8097	0.0424	-1.4725	30.6	12.0	156.3	3.4	7.23	0.74
D	800	1.021	0.0398	0.3578	337.0	12.8	90.1	7.1	5.29	0.08
E	850	1.128	0.0377	0.2023	1002.7	13.5	95.1	18.6	6.18	0.03
F	875	1.098	0.0376	0.1174	1073.2	13.6	97.2	30.8	6.15	0.03
G	925	1.145	0.0365	0.0741	3495.3	14.0	98.4	71.1	6.49	0.02
H	975	1.186	0.0396	0.0930	2346.8	12.9	98.0	98.1	**6.71**	**0.02**
I	1100	2.775	0.0510	0.4621	151.2	10.0	95.2	100.0	15.38	0.17
total gas age			n=9		8738.5	13.4			6.50	0.06*
9189 Nancy, 15.10 mg cryptomelane, J = 0.0032204, D = 1.00661, NM-104, Lab# = 50227-01										
A	600	30.44	0.0418	102.6	567.2	12.2	0.4	5.5	0.69	1.47
B	700	1.180	0.0362	0.8383	589.5	14.1	80.4	11.2	5.40	0.05
C	750	1.076	0.0356	-0.3296	54.1	14.3	110.3	11.8	6.74	0.32
D	800	1.022	0.0369	0.1987	1294.0	13.8	95.3	24.6	5.52	0.03
E	850	1.089	0.0341	0.1104	1573.0	15.0	97.6	39.9	6.04	0.02
F	875	1.113	0.0328	0.0937	1092.4	15.6	97.9	50.6	6.19	0.03
G	925	1.133	0.0327	0.0795	4994.4	15.6	98.2	98.7	**6.33**	**0.02**
H	975	1.056	0.0294	-3.2346	18.3	17.4	193.1	98.9	11.55	0.89
I	1025	1.384	0.0290	0.7116	89.2	17.6	85.0	99.9	6.71	0.19
J	1075	2.563	0.0367	-1.0969	8.09	13.9	113.3	100.0	16.64	2.36
total gas age			n=10		10280.1	15.0			5.83	0.22*

TABLE 2—continued.

ID	Temp (°C)/watts	$^{40}Ar/^{39}Ar$	$^{37}Ar/^{39}Ar$	$^{36}Ar/^{39}Ar$	$^{39}Ar_K$ (x 10^{-3})	K/Ca (x 10^{-16} mol)	$^{40}Ar^*$ (%)	^{39}Ar (%)	Age (Ma)	±1σ (Ma)
9189 Nancy, 3.6 mg cryptomelane, J = 0.0032462, D = 1.00676, NM-104, Lab# = 50226-02										
A	3	16.51	0.0372	55.10	166.5	13.7	1.8	6.1	1.71	0.66
B	7	1.227	0.0288	0.9530	581.4	17.7	78.2	27.5	5.51	0.04
C	10	1.151	0.0284	0.3715	982.4	18.0	91.0	63.5	6.00	0.03
D	13	1.170	0.0272	0.3810	761.1	18.8	90.7	91.5	**6.08**	**0.03**
E	16	1.265	0.0269	0.8487	184.4	18.9	80.3	98.2	5.83	0.10
F	20	1.898	0.0209	3.463	34.0	24.4	45.8	99.5	5.02	0.54
G	22	4.660	-0.0184	14.12	9.23	-	10.1	99.8	2.74	1.84
H	24	11.90	-0.1336	38.91	5.03	-	3.1	100.0	2.15	3.46
total gas age			**n=8**		2724.2	17.9			5.62	0.18*

TABLE 3—Argon isotopic results for single crystal sanidine total fusion analysis. Isotopic ratios corrected for blank, radioactive decay, and mass discrimination, not corrected for interfering reactions. Individual analyses show analytical error only; weighted mean age errors include error in J and irradiation parameters. n= number of heating steps; **K/Ca** = molar ratio calculated from reactor produced $^{39}Ar_K$ and $^{37}Ar_{Ca}$; *= 2σ error; ****** MSWD outside 95% confidence interval; **D** = mass spectrometer discrimination value.

ID	$^{40}Ar/^{39}Ar$	$^{37}Ar/^{39}Ar$	$^{36}Ar/^{39}Ar$	$^{39}Ar_K$ (x 10^{-3})	K/Ca (x 10^{-15} mol)	$\%^{40}Ar^*$	Age (Ma)	± 1 σ (Ma)
RC-KM-28, single crystal sanidine, J = 0.0014699, D = 1.00712, NM-152, Lab# = 53216								
02	4.218	0.0057	0.2510	4.46	89.1	98.3	10.96	0.06
11	4.992	0.0070	2.847	9.17	73.4	83.2	10.97	0.05
01	4.207	0.0077	0.1849	9.28	66.3	98.7	10.98	0.04
09	4.221	0.0067	0.2295	6.26	75.6	98.4	10.98	0.05
13	4.214	0.0064	0.1862	9.67	79.6	98.7	11.00	0.03
07	4.202	0.0059	0.1397	5.27	85.8	99.0	11.00	0.04
14	4.236	0.0060	0.2344	2.76	85.3	98.4	11.02	0.09
08	4.190	0.0071	0.0655	6.17	72.3	99.6	11.03	0.05
03	4.450	0.0143	0.9349	7.54	35.6	93.8	11.04	0.05
12	4.625	0.0087	1.492	9.86	58.8	90.5	11.06	0.05
04	4.239	0.0061	0.1660	5.99	83.6	98.9	11.08	0.04
06	4.391	0.0071	0.6619	12.8	71.4	95.6	11.09	0.03
05	4.221	0.0060	0.0260	14.6	85.5	99.8	11.14	0.03
10	4.272	0.0058	0.1534	7.41	87.5	99.0	11.17	0.04
weighted mean MSWD = 2.9** n=14					75.0 ± 14.4		11.05	0.05*

studies that poorly crystalline, low K cryptomelane undergoes phase transformations and thus possibly Ar loss at much lower temperatures than high K, crystalline cryptomelane. We suggest that the analyzed samples contain a small percentage of low crystallinity cryptomelane that is at least partially responsible for the Ar loss that we see. It is also possible that the high crystallinity cryptomelane was precipitated over a period of time, and the gentle increase in ages seen over the majority of the age spectra actually records the precipitation history of the cryptomelane. The ages determined for these samples are in complete agreement with field data and isotopic ages that constrain the age of mineralization between 7.4 Ma and 3.7 Ma (Chamberlin and Eggleston 1996; Dunbar and Miggins 1996; and Chamberlin 1999).

Manganese mineralization and the red zone alteration

Eggleston et al. (1983b) interpreted the red zone (Fig. 1D) as a relatively small epithermal zone locally overprinted on the southeast margin of a broad regional zone of potassium metasomatism. Because the red zone was found to be strongly depleted in manganese and centrally located, it was hypothesized as the likely source area for surrounding epithermal manganese oxide veins that compose the Luis Lopez district (see Eggleston et al. 1983a; Fig. 5). Recent mapping and $^{40}Ar/^{39}Ar$ dating of rhyolite dikes in the district (Chamberlin and Eggleston 1996; Chamberlin et al. 2002; Chamberlin et al. 2004 this volume) do not support this earlier interpretation.

An east-trending rhyolite dike (RC-KM-28) is distinctly unaltered (contains fresh glassy plagioclase, clear sanidine, and black biotite) where it cuts across the zone of red alteration in the Hell Mesa Tuff. Sanidine from this dike is dated at 11.05 ± 0.05 Ma (Table 3; Fig. 6). A compositionally and texturally equivalent coarsely porphyritic rhyolite plug that intrudes caldera-facies of Hells Mesa Tuff near Red Canyon (Fig. 1) yields a precise $^{40}Ar/^{39}Ar$ age 10.99 ± 0.06 Ma from sanidine phenocrysts (Chamberlin et al. 2004 this volume). The contact of this nearly contiguous dike with the plug is obscured by colluvium although the age and petrologic relationships indicate the plug and dike are part of the same intrusion. The rhyolite plug occurs in the footwall of the range-bounding fault zone and is locally cut by manganese veins and shows evidence of potassium metasomatism (Eggleston 1982; Chamberlin and Eggleston 1996). Fine-grained phenocryst-poor rhyolite dikes of late Oligocene age (ca. 28.5–28.7 Ma) are potassically altered (contain secondary biotite) where they cut red hematized Hells Mesa Tuff south of the Nancy mine (Chamberlin and Eggleston 1996; Chamberlin et al. 2004 this volume). These observations indicate that the red alteration zone is younger than 28.5 Ma and older than 11.0 Ma and cannot be the source of manganese mineralization dated at 6.7–6.3 Ma.

Manganese mineralization and potassium metasomatism

The relationship between manganese mineralization and regional potassium metasomatism remains speculative. Although not economically significant, manganese mineralization in the Magdalena Mountains, west of the Luis Lopez district, is nearly as widespread as potassium metasomatism and appears to occur in proximity to metasomatized rocks (cf. Farnham 1961; Dunbar et al. 1994). Several large areas of potassium metasomatism in the Basin and Range province are spatially related to Tertiary volcanic centers in strongly extended terranes and Miocene basins (Chapin and Lindley 1986). Manganese districts are also commonly associated with these large K_2O anomalies in the Basin and Range (Chapin and Glazner 1983; Chapin and Lindley 1986).

Ages of potassium metasomatism in the Socorro region, as determined by $^{40}Ar/^{39}Ar$ methods, range from 14.1 Ma at Water Canyon, 15 km west of the study area, to 7.4 Ma at Box Canyon, about 3 km north of the Nancy/Tower mine (Dunbar and Miggins 1996). The minimum age for manganese mineralization in the Luis Lopez district (6.7 Ma) is slightly younger than local potassium metasomatism (7.4 Ma). These isotopic age relationships are strongly support-

ed by field observations of manganese veins that consistently cut metasomatized and jasperized rocks. Geochemical studies have shown that tuffs and lavas in the Socorro–Magdalena K_2O anomaly are typically depleted in Na, Ca, Mg, Sr, and Mn (Chapin and Lindley 1986; Dunbar et al. 1994; Ennis et al. 2000). Although speculative, the available data would permit the eastern part of the Socorro–Magdalena K_2O anomaly to be a source area for slightly younger manganese mineralization in the Luis Lopez district.

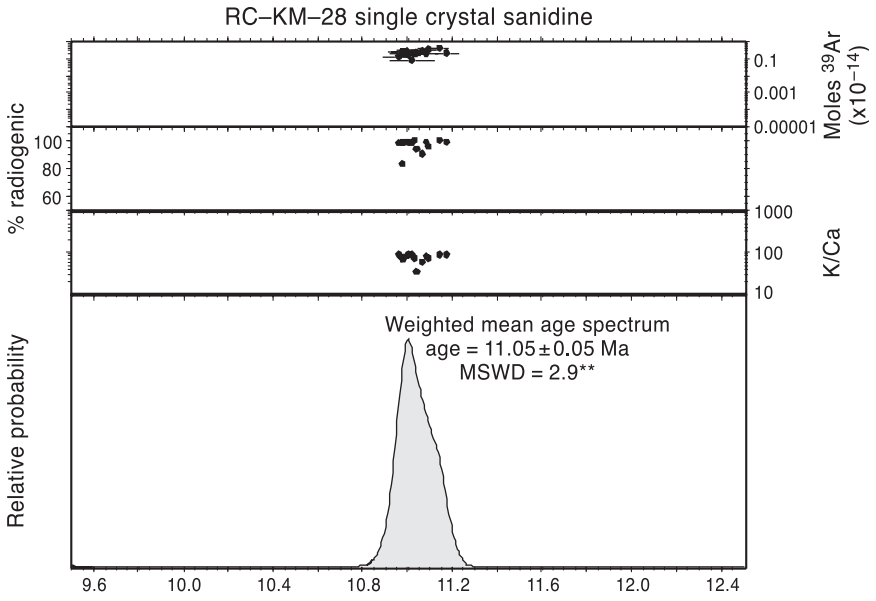

FIGURE 6—Age probability distribution diagram for sample RC-KM-28 single crystal sanidine total fusion analysis. * 2σ ** MSWD outside 95% confidence interval.

A conceptual model for manganese mineralization

Timing constraints for manganese mineralization in the Luis Lopez district suggest that upper crustal magmatism (as expressed by silicic volcanism), potassium metasomatism and ore mineralization are interrelated. Based on these constraints, we propose the following mineralization model for the district. Our preliminary model incorporates many of the features proposed by Eggleston et al. (1983a) and only abandons the need for the red zone to be the area for the source of manganese. Instead, our system is laterally associated with silicic magmatism similar in age to the cryptomelane analyzed during this study (Fig. 7).

The youngest silicic volcanism in proximity to the study area is located west of Socorro Peak and approximately 9 km north-northeast of the Nancy mine. The age of this magmatism is slightly older than mineralization. Silicic volcanism at Socorro Peak began with eruption of several small flat-topped dacitic domes (tortas) at 9.5 Ma (Newell 1997; Chamberlin 1999). Rhyolite lava dome eruptions were then sequentially emplaced in this area at 8.7, 7.8, 7.5, and 7.0 Ma (Newell 1997). Rhyolite volcanism was immediately followed by eruption of a xenocrystic trachyandesite lava on the west flank of the Socorro Mountains (Sedillo Hill) at 6.9 Ma (McIntosh and Chamberlin unpublished data). This extended period of silicic volcanism is interpreted here as the surface expression of the emplacement of a composite upper-crustal pluton under the Socorro Peak area in Late Miocene time. A hybrid trachyandesite magma, containing partially assimilated sanidine xenocrysts, represents the last thermal replenishment of this upper crustal magmatic system at 6.9 Ma. Without magmatic replenishment, upper-crustal silicic plutons must become completely crystalline and cooled by hydrothermal circulation within a few hundred thousand years after their emplacement (Lachenbruch et al. 1976) Approximately 0.5 m.y. can be subtracted from the eruption age of local episodes of silicic volcanism in order to estimate the probable minimum age of each associated hydrothermal event (Lipman et al. 1976). Long-lived hydrothermal systems at young ignimbrite calderas (> 1 Ma) suggest that periodic replenishment of crustal magmatic systems is a common phenomenon (Lipman 2000). We suggest that an upper crustal composite pluton of granitic composition associated with the Socorro Peak rhyolite lava domes is the most likely source of heat energy to drive the hydrothermal system at Luis Lopez.

In our model the Luis Lopez district lies on the outer margin of a hydrothermal system centered near Socorro Peak. The presence of precious metal sulfide mineralization at the Torrance mine (Socorro Peak district; Lasky 1932) is more

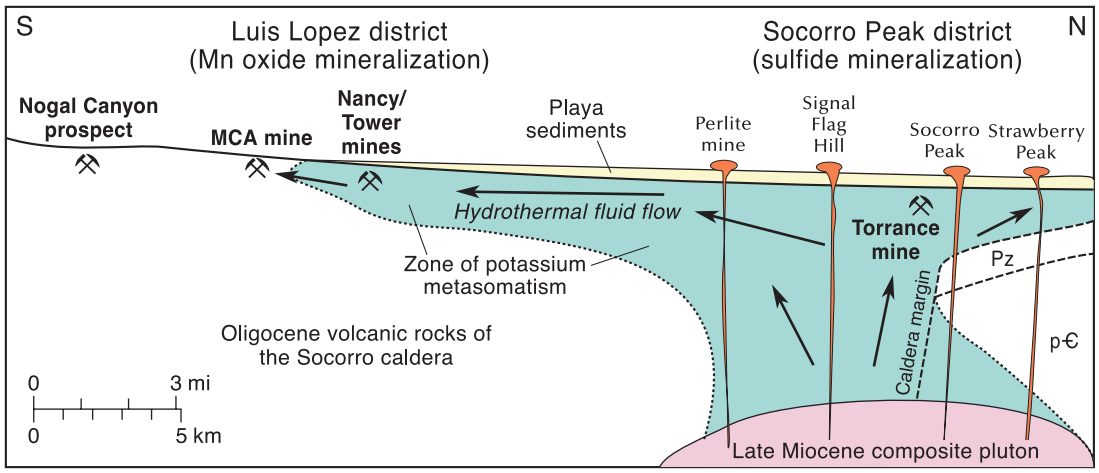

FIGURE 7—A schematic model for mineralization and alteration in the Luis Lopez manganese district. Figure based on diagrammatic cross section of Eggleston et al. (1983b) with modifications from Chamberlin (1999) and Chamberlin et al. (2002).

typical of mineralization proximal to a heat source. Higher overall fluid inclusion homogenization temperatures at the Nancy/Tower mines when compared to the MCA mine (Norman et al. 1983) support a temperature gradient from north to south. A thick sequence of playa claystones in the upper Popotosa Formation (Figs. 1,7) essentially serves as an impermeable cap on the hydrothermal system. As the hydrothermal fluids emerged from under this cap, boiling and mineralization occurred. In this scenario the Luis Lopez manganese deposits represent distal mineralization and are analogous to argentiferous manganese oxide mineralization associated with base metal sulfide mineralization in some manto deposits of northern Mexico (Megaw 1990).

The patterns of mineralization and alteration expected in our model suggest that potassium metasomatism is a product of a hydrothermal system similar to the original interpretation of D'Andrea-Dinkelman et al. (1983). Both manganese mineralization and alteration appear linked to north-south faults that apparently served as fluid conduits in the study area, as indicated by the observation that virtually all bedrock faults northeast of the Nancy mine are filled with jasperoidal silica (Chamberlin 1999; Chamberlin et al. 2002). Although older ages for potassium metasomatism have been determined west of the district (14.1 Ma at Water Canyon, Dunbar and Miggins 1996), we suggest that the Water Canyon episode of alteration is associated with an entirely separate hydrothermal system of middle Miocene age (cf. Newell 1997). Initial age dating of manganese mineralization, similar in character to Luis Lopez, in the southern Magdalena Mountains supports this hypothesis. Studies are continuing to document these relationships.

Conclusions

The results of $^{40}Ar/^{39}Ar$ analysis of cryptomelane from two deposits in the Luis Lopez manganese district agree with age estimates based on geologic relationships established by previous workers. Mineralization in the entire district is nearly contemporaneous based on the similarity of ages, coupled with the wide separation (geographic and stratigraphic) of the MCA (6.69 ± 0.04 Ma, minimum age) and the Nancy (6.33 ± 0.04 Ma, minimum age) mines. The timing of mineralization is coincident with the waning of upper crustal silicic magmatism in the Socorro Peak area (8.7–7.0 Ma), which represents the most likely heat source for the hydrothermal system. Timing relationships with respect to the regional potassic metasomatism indicate the manganese mineralization (~ 6.7 Ma) is slightly younger than metasomatism (7.4 Ma; Dunbar and Miggins 1996) although they may be interrelated.

Acknowledgments

We would like to thank Drs. Andrew Campbell, William McIntosh, and Matthew Heizler for their constructive reviews of the manuscript. Richard Esser provided assistance with the Ar analysis. Chris McKee assisted with the X-ray diffraction analysis. The New Mexico Bureau of Geology and Mineral Resources, Dr. Peter Scholle, Director and State Geologist, supported this work.

References

Cather, S. M., Chamberlin, R. M., Chapin, C. E., and McIntosh, W. C., 1994, Stratigraphic consequences of episodic extension in the Lemitar Mountains, central Rio Grande rift; *in* Keller, G. R., and Cather, S. M. (eds.), Basins of the Rio Grande rift—structure, stratigraphy, and tectonic setting: Geological Society of America, Special Paper 291, pp. 157–170.

Chamberlin, R. M., 1980, Cenozoic stratigraphy and structure of the Socorro Peak volcanic center, central New Mexico: Unpublished Ph.D. thesis, Colorado School of Mines, 495 pp.

Chamberlin, R. M., 1983, Cenozoic domino-style crustal extension in the Lemitar Mountains, New Mexico—a summary; *in* Chapin, C. E., and Callender, J. F. (eds.), Socorro region II: New Mexico Geological Society, Guidebook 34, pp. 111–118.

Chamberlin, R. M., 1999, Preliminary geologic map of the Socorro quadrangle, Socorro County, New Mexico: New Mexico Bureau of Mines and Mineral Resources, Open-file Geologic Map OF-GM-34, 46 p.

Chamberlin, R. M., and Eggleston, T. L., 1996, Geologic map of the Luis Lopez 7.5 minute quadrangle, Socorro County, New Mexico: New Mexico Bureau of Mines and Mineral Resources, Open-file Report 421, 152 pp.

Chamberlin, R. M., Eggleston, T. L., and McIntosh, W. C., 2002, Geology of the Luis Lopez 7.5-minute quadrangle, Socorro County, New Mexico: New Mexico Bureau of Geology and Mineral Resources, Open-file Geologic Map, OF-GM-53, 46 pp., 2 sheets.

Chamberlin, R. M., McIntosh, W. C., and Eggleston, T. L., 2004 this volume, $^{40}Ar/^{39}Ar$ Geochronology and eruptive history of the eastern sector of the Oligocene Socorro caldera, central Rio Grande rift, New Mexico; *in* Cather, S. M., McIntosh, W. C., and Kelley, S. A. (eds.), Tectonics, geochronology, and volcanism in the Southern Rocky Mountains and Rio Grande rift: New Mexico Bureau of Geology and Mineral Resource, Bulletin 160, pp. 251–280

Chapin, C. E., and Cather, S. M., 1994, Tectonic setting of the axial basins of the northern and central Rio Grande rift; *in* Keller, G. R., and Cather, S. M. (eds.), Basins of the Rio Grande rift—structure, stratigraphy, and tectonic setting: Geological Society of America, Special Paper 291, pp. 5–25.

Chapin, C. E., and Glazner, A. F., 1983, Widespread K_2O metasomatism of volcanic and sedimentary rocks in the southwestern United States: (abs.): Geological Society of America, Abstracts with Programs, v. 15, no. 5, p. 282.

Chapin, C. E., and Lindley, J. I., 1986, Potassium metasomatism of igneous and sedimentary rocks in the detachment terranes and other sedimentary basins—economic implications; *in* Beatty, B., and Wilkinson, P. A. K. (eds.), Frontiers in geology and ore deposits of Arizona and the Southwest: Arizona Geological Society Digest, v. 16, pp. 118–126.

Chuchrov, F. V., Shanin, L. L., and Yermilova, L. P., 1966, Feasibility of absolute-age determination for potassium-carrying manganese minerals: International Geology Review, v. 8, pp. 278–280.

D'Andrea-Dinkelman, J. F., Lindley, J. I., Chapin, C. E., and Osburn, G. R., 1983, The Socorro K_2O anomaly—a fossil geothermal system in the Rio Grande rift; *in* Chapin, C. E., and Callender, J. F. (eds.), Socorro region II: New Mexico Geological Society, Guidebook 34, pp. 76–77.

Deino, A., and Potts, R., 1990, Single-crystal $^{40}Ar/^{39}Ar$ dating of the Olorgesailie Formation, Southern Kenya rift: Journal Geophysical Research, v. 95, no. B6, pp. 8453–8470.

Dunbar, N. W., and Miggins, D., 1996, Chronology and thermal history of potassium metasomatism in the Socorro, New Mexico, area—evidence from $^{40}Ar/^{39}Ar$ dating and fission track analysis (abs.): New Mexico Geology, v. 18, no. 2, pp. 50–51.

Dunbar, N. W., Chapin, C. E., Ennis, D. J., and Campbell, A. R., 1994, Trace element and mineralogical alteration associated with moderate and advanced degrees of K-metasomatism in a rift basin at Socorro, New Mexico; *in* Chamberlin, R. M., Kues, B. S., Cather, S. M., Barker, J. M., and McIntosh, W. C. (eds.), Mogollon slope: New Mexico Geological Society, Guidebook 45, pp. 225–231.

Eggleston, T. L., 1982, Geology of the central Chupadera Mountains, Socorro County, New Mexico: New Mexico Bureau of Mines and Mineral Resources, Open-file Report 141, 162 p.

Eggleston, T. L., Osburn, G. R., and Chapin, C. E., 1983a, Third day road log from Socorro to San Antonio, Nogal Canyon, Chupadera Mountains, Luis Lopez manganese district, and the MCA mine; *in* Chapin, C. E., and Callender, J. F. (eds.), Socorro region II: New Mexico Geological Society, Guidebook 34, pp. 61–79.

Eggleston, T. L., Norman, D. I., Chapin, C. E., and Savin, S., 1983b, Geology, alteration, and genesis of the Luis Lopez manganese district, New Mexico; *in* Chapin, C. E., and Callender, J. F. (eds.), Socorro region II: New Mexico Geological Society, Guidebook 34, pp. 241–246.

Ennis, D. J., 1996, The effects of K-metasomatism on the mineralogy and geochemistry of silicic ignimbrites near Socorro, New Mexico: Unpublished M.S. thesis, New Mexico Institute of

Mining and Technology, 160 pp.
Ennis, D. J., Dunbar, N. W., Campbell, A. R., and Chapin, C. E., 2000, The effects of K-metasomatism on the mineralogy and geochemistry of silicic ignimbrites near Socorro, New Mexico: Chemical Geology, v. 167, no. 3-4, pp. 285–312.
Farnham, L. L., 1961, Manganese deposits of New Mexico: U.S. Bureau of Mines, Information Circular 8030, 176 pp.
Hénocque, O., Ruffet, G., Colin, F., and Féraud, G., 1998, $^{40}Ar/^{39}Ar$ dating of West African lateritic cryptomelanes: Geochimica et Cosmochimica Acta, v. 62, no. 16, pp. 2739–2756.
Hewett, D. F., 1964, Veins of hypogene manganese oxide minerals in the southwestern United States: Economic Geology, v. 59, no. 8, pp. 1429–1472.
Lachenbruch, A. H., Sorey, M. I., Lewis, R. E., and Sass, J. H., 1976, The near-surface hydrothermal regime of Long Valley caldera: Journal of Geophysical Research, v. 81, no. 5, pp. 763–784.
Lasky, S. G., 1932, The ore deposits of Socorro County, New Mexico: New Mexico Bureau of Geology and Mineral Resources, Bulletin 8, 139 pp.
Lipman, P. W., 2000, Calderas; *in* Sigurdsson, H., Houghton, B., McNutt, S., Rymer, H., and Stix, J. (eds.), Encyclopedia of volcanoes: Academic Press, San Diego, pp. 643–662.
Lipman, P. W., Fisher, F. S., Mehnert, H. H., Naeser, C. W., Luedke, R. G., and Steven, T. A., 1976, Multiple ages of middle-Tertiary mineralization and alteration in the western San Juan Mountains, Colorado: Economic Geology, v. 71, no. 3, pp. 371–588.
Mahon, K. I., 1996. The New "York" regression—application of an improved statistical method to geochemistry: International Geology Review, v. 38, no. 4, pp. 293–303.
Megaw, P. K. M., 1990, Geology and geochemistry of the Santa Eulalia mining district, Chihuahua, Mexico: Unpublished Ph.D. dissertation, University of Arizona, 549 pp.
Miesch, A. T., 1956, Geology of the Luis Lopez manganese district, Socorro County, New Mexico: New Mexico Bureau of Mines and Mineral Resources, Circular 38, 31 pp.
Newell, H. H., 1997, $^{40}Ar/^{39}Ar$ geochronology of Miocene silicic lavas in the Socorro–Magdalena area, New Mexico: Unpublished M.S. thesis, New Mexico Institute of Mining and Technology, 190 pp.
Newell, H. H., Kyle, P. R., and McIntosh, W. C., 1996, $^{40}Ar/^{39}Ar$ dating of Miocene silicic lavas of the Socorro–Magdalena area (abs.): New Mexico Geology, v. 18, no. 2, p. 50.
Norman, D. I., Bazrafshan, K., and Eggleston, T. L., 1983, Mineralization of the Luis Lopez epithermal manganese deposits in light of fluid inclusion and geologic studies; *in* Chapin, C. E., and Callender, J. F. (eds.), Socorro region II: New Mexico Geological Society, Guidebook 34, pp. 247–251.
Osburn, G. R., Petty, D. M., Chamberlin, R. M., and Roth S. J., 1986 (revision of 1981 report), Geology of the Molino Peak Quadrangle: New Mexico Bureau of Mines and Mineral resources, Open-file Report 139a, 57 p.
Samson, S. D., and, Alexander, E. C., Jr., 1987, Calibration of the interlaboratory $^{40}Ar/^{39}Ar$ dating standard, Mmhb-1: Chemical Geology, v. 66, no. 1–2, pp. 27–34.
Steiger, R. H., and Jäger, E., 1977, Subcommission on geochronology—convention on the use of decay constants in geo- and cosmochronology: Earth and Planetary Science Letters, v. 36, pp. 359–362.
Taylor, J. R., 1982, An introduction to error analysis—the study of uncertainties in physical measurements: University Science Books, Mill Valley, Calif., 270 pp.
U.S. Department of Energy, 1979a, Aerial radiometric and magnetic survey, Tularosa National topographic map, New Mexico: U.S. Department of Energy, Open-file Report GJBX-67 (79), v. 2, (includes aeroradiometric data for K, U, and Th along 33 flight lines).
U.S. Department of Energy, 1979b, Aerial radiometric and magnetic survey, Socorro National topographic map, New Mexico: U.S. Department of Energy, Open-file Report GJBX-163 (79), v. 2, (includes aeroradiometric data for K, U, and Th along 33 flight lines).
Vasconcelos, P. M., 1999, K-Ar and $^{40}Ar/^{39}Ar$ geochronology of weathering processes: Annual Reviews in Earth and Planetary Sciences, v. 27, pp. 183–229.
Vasconcelos, P. M., 2000, $^{40}Ar/^{39}Ar$ geochronology of supergene processes in ore deposits; *in*, Lambert, D. D., and Ruiz, J. (eds.), Application of radiogenic isotopes to ore deposit research and exploration: Reviews in Economic Geology, v. 12, pp. 73–113.
Willard, M. E., 1973, Geology of the Luis Lopez manganese district, New Mexico: New Mexico Bureau of Mines and Mineral Resources, Open-file Report 186, 81 pp.
York, D., 1969, Least squares fitting of a straight line with correlated errors: Earth and Planetary Science Letters, v. 5, no. 5, pp. 320–324.